Cite this article
Masters I, Bird J, Birch B *et al.* (2022)
Remote river energy system: an open-source low-maintenance turbine design for remote areas.
Proceedings of the Institution of Civil Engineers – Energy **175(2)**: 64–80,
https://doi.org/10.1680/jener.21.00101

Research Article
Paper 2100101
Received 13/09/2021;
Accepted 22/09/2021;
Published online 16/03/2022

Energy

ice Publishing

Remote river energy system: an open-source low-maintenance turbine design for remote areas

Ian Masters PhD
College of Engineering, Swansea University, Swansea, UK
(corresponding author: i.masters@swansea.ac.uk)

Joshua Bird MEng
College of Engineering, Swansea University, Swansea, UK

Benjamin Birch MEng
College of Engineering, Swansea University, Swansea, UK

Maximilian Reader MEng
College of Engineering, Swansea University, Swansea, UK

William Turner MEng
College of Engineering, Swansea University, Swansea, UK

Tom Holland MEng
College of Engineering, Swansea University, Swansea, UK

Thomas Lake PhD
College of Engineering, Swansea University, Swansea, UK

Alison J. Williams PhD
College of Engineering, Swansea University, Swansea, UK

Axial flow hydro-kinetic turbines convert the kinetic energy of a flowing fluid into electrical energy, and can be designed for deployment in a wide range of locations. As relatively recent technology, these designs are often high in cost, complex and require specialist maintenance and materials. This is not viable for many communities in developing countries, which may subsequently remain reliant on fossil fuels. A remote river energy system has been designed to be built and maintained using minimal equipment, with components that can be readily obtained. A formal design process has been used with design review and feedback stages; design tools included Simulink modelling, finite-element analysis, computational fluid dynamics, nodal analysis and flume testing. A handful of components such as the turbine blades require specialist machining and maintenance. Results demonstrate how an effective water turbine with a 3 kW output can be theoretically produced and maintained without an over-reliance on specialised components and tools, thereby producing a more economically viable water turbine for use in developing countries. Open-source distribution of the design drawings will facilitate application of the design and improvements by other stakeholders. The design study presented is a platform for prototype technology trials to further develop the concept.

Keywords: renewable energy/sustainability/UN SDG 7: Affordable and clean energy

Notation

A	area (m^2)
A_b	Bolt nominal diameter (mm)
A_c	crank angle (rad/s)
B	pad length (m)
b	pad width (m)
C	average diametral clearance (in.; 1 in. = 2.54 cm)
C_D	coefficient of drag (dimensionless)
C_f	coefficient of thrust (dimensionless)
C_L	coefficient of lift (dimensionless)
C_P	coefficient of power (dimensionless)
C_T	coefficient of torque (dimensionless)
D_1	inner bearing diameter (m)
D_2	outer bearing diameter (m)
d_{piston}	piston diameter (mm)
F_b	tensile bolt force (N)
F_D	drag force (N)
F_L	lift force (N)
F_N	normal force (N)
F_r	friction force (N)
f	friction factor (dimensionless)
G	groove width (m)
H_{jo}	journal bearing power loss (W)
H_{th}	thrust bearing power loss (W)
i	number of pads (dimensionless)
J	polar moment of inertia (m^4)
k_g	pad/circumference ratio (dimensionless)
L_{jo}	journal bearing length (m)
l_c	crank rod length (mm)
M	horsepower per square inch (hp/$in.^2$; 1 $in.^2$ = 6.45 cm^2)
P_{jo}	radial load capacity (Pa)
P_{th}	pressure bearing capacity (Pa)
r	blade radius (m)

r_c	crank radius (mm)
T_f	torque friction (N)
T_m	mechanical torque (N m)
T_p	pump torque (N m)
t_{jo}	bearing thickness (in.)
U	river velocity (m/s)
U_d	pitch diameter peripheral speed (m/min)
$\dot{V}_p$	pump volume flow (m^3/s)
v_{piston}	piston velocity (mm/s)
W_{jo}	maximum vertical (weight) load (N)
W_{th}	maximum thrust load (N)
x_{piston}	piston position (mm)
η	lubricant viscosity (Pa s)
θ_r	river turbine angle (rad/s)
μ	coefficient of friction (dimensionless)
ρ	density of water (kg/m^3)
ρ_{part}	density of part (kg/m^3)
σ_b	Bolt stress (Pa)
Ψ	power (W)
ω_r	river turbine angular velocity (rad/s)
ω_{rev}	shaft rotational speed (r/min)

1. Introduction

Globally, countries are attempting to increase energy supply capacity while ensuring that any energy solution is reliable and affordable for all people (The World Bank Group, 2009). This paper describes a contribution to that effort: the design of a product capable of harnessing energy from a river to be implemented in remote access locations, a remote river energy system (RRES). The concept generates electricity using a water current turbine that drives a dual-action piston pump, pumping water to an on-shore hydro-electric generator. Emphasis is placed on the installation and repair facilities that would likely be present in developing communities, and how these communities would have to interface with the turbine without any external aid, such as with self-repair.

Sustainability is defined as meeting the world's present needs without compromising future generations and includes the key concept that the essential needs of the world's poor must be met with all priority (UN, 1987). The UN Sustainable Development Goals also include access to affordable and clean energy for all, and making cities and human settlements sustainable (Griggs *et al*., 2013). Therefore there is a definite need for an inexpensive device capable of generating electricity off-grid for poor communities that minimises the time and resources required over the device's operational life.

High costs hinder the progress and deployment of remote river turbines (Kirke, 2019). Minimising the number of components, manufacturing processes and business costs are key considerations throughout this paper in order to mitigate these high costs. As such, it is proposed that the turbine drawings will be published open source. The use of an open-source license will mean the turbine can be made anywhere, by anybody; enabling the potential for rapid deployment of the turbine all over the world. Remote communities and people groups could then build their own turbine and generate decentralised electricity, in an inexpensive manner. The designs will be distributed in a format that conforms to the standards for redistribution outlined in the Open Source Hardware Association definition (OSHWA, 2020).

2. Literature review

Floating river and canal turbines are emerging technology. One well-distributed and published example is the 'Smart Monofloat' from Smart Hydro Power (Smart Hydro Power, 2015). The same company has also developed a turbine system which can be positioned on the river bed (Smart Hydro Power, 2016). The Smart Monofloat is a very similar design concept to the design proposed here; however, it is very heavily engineered. This means that it requires complete manufacture in a factory, followed by deployment to the required location.

The Ocean Renewable Power Company (ORPC) (ORPC, 2020a) has designed generation systems that are fixed to the river bed. The ORPC systems are larger than the proposed RRES design, and are designed to fulfil a different electrical demand, such as a relatively large settlement in Alaska (ORPC, 2020b), rather than to smaller and off-grid communities. Designs have also been developed for small communities that harness wave power, for example (Castro and Chiang, 2020).

Alternatives suitable for use in remote locations include solar power and small-scale wind power (Razmjoo *et al*., 2019). Solar power is most useful nearer the equator (Boddapati and Daniel, 2020). Wind power offers a good method for larger open spaces (Al-Bahadly, 2009). However, if the proposed location is heavily forested or in a valley, it may not get enough wind or clear enough access to the sun, which are required to provide continual power (Anyi *et al*., 2010; Bansal *et al*., 2005; Tong, 2010), and multiple renewable sources could provide a solution. Additionally, river or tidal systems could be used in high-latitude locations as there is very limited exposure to sunlight for solar power during winter.

While there are pre-existing river turbines with similar designs and purpose to the proposed design, they require complex and specialist manufacturing techniques (ORPC, 2020a; Smart Hydro Power, 2015). The blades and specialist components of the RRES could be purchased from a supply company, but the rest of the design can be manufactured in an inexpensive way, reducing overall capital cost. Designing the turbine for a minimal number of moving parts (Orme and Masters, 2005)

should reduce the need for expensive installation and maintenance.

3. Design overview

The goal of an easy-to-repair, robust system was formalised into the design specification shown in Table 1. Offshore, the RRES is a stationary floating platform which suspends a two-blade turbine in the flow of the river. The platform is held in situ by two submerged cables which can be used to angle the turbine directly into the flow. The platform comprises a chassis constructed from C and L beams, which can be coated in a corrosion-resistant paint, and decommissioned barrels; as shown in Figure 1. The bow at the front aids buoyancy, especially in higher-flow-rate scenarios. The power output of the generator and other parameters across the operational river velocities can be seen in Figure 2. A series of iterations of rotor diameter and rated power was made, using the overall maximum lifting weight as a constraint, resulting in a 3.6 m dia. rotor producing 3 kW electrical output (after losses) at a rated river speed of 1.76 m/s. This is a compromise between capturing energy efficiently at a range of flow speeds without the excess structural costs that would be required to continue generating at higher, infrequently occurring, flow speeds.

Table 1. Device specification

1. Mechanical	
1.1	Support own weight in transit and installation
1.2	Weight limit of 2000 kg to minimise size of crane
1.3	Neutrally buoyant blades/shaft
1.4	Designed to operational load cases
2. Operating conditions	
2.1	Function at river velocities between 1 and 4 m/s
2.2	Shut off at 4 m/s
2.3	Temperatures between 5 and 34°C
2.4	Fresh water
2.5	Resist corrosion
3. Manufacture	
3.1	Minimise use of novel materials
3.2	Minimise use of advanced manufacturing methods
3.3	Must be designed for low-cost repair
3.4	Must be designed without seals underwater
4. Maintenance	
4.1	Wet service[a] every 6 months
4.2	Dry service[b] every 2.5 years
4.3	Must support two people for wet service
4.4	Must be safe to approach and transfer from a boat
4.5	Must be able to be lifted by a crane
4.6	All seals must be accessible in wet service
4.7	All electronics must be onshore
5 Health and safety	
5.1	Design must follow BSI[c] and ISO[c] standards
5.2	Manufacture must adhere to local legislation
5.3	Maintenance must observe local safe working practices
5.4	All components will use an SF[c] of 2 unless stated otherwise
5.5	River turbine blades will have an SF of 3.3
5.6	Chassis will have an SF of 1.8

[a]Wet service will leave the turbine in location
[b]Dry service will include lifting the turbine from the water
[c]BSI, British Standards Institution; ISO, International Organization for Standardization; SF, safety factor

The blades are made using a fibreglass shell to create the profile and a central steel spar for stiffness. The blades, hub and shaft are filled with closed-cell foam to ensure neutral buoyancy when in the river, as per the specification in Table 1. They harness energy in the river by turning a gear system to actuate the power take off (PTO) system, comprising a dual-action piston pump and one-way valves. The use of a gear system avoids the need for a chain or belt drive, which would be more susceptible to damage and wear.

The PTO pumps water to the onshore 3 kW hydro-electric generator through a closed-loop system (Figure 1). The use of a closed-loop water system allows all of the electronics to be kept onshore, in accordance with the design specification, avoiding expensive submerged electrical cables. A closed-loop control system is used to operate a throttling valve which regulates the flow of water. This keeps the pump flow within operating conditions of the generator and stops the blades if the river flow exceeds 4 m/s.

The turbine is installed by lifting it into the river using a truck-mounted crane, then towing it into position with a boat and fixing the two mooring lines. The device is designed to be sited up to 200 m from the shore. An in situ inspection and wet service would be required every 6 months. As all offshore components are mechanical, with all electrical components being on shore, the servicing process is simplified and safer to carry out. During this service, the turbine blades would be stopped using the on-shore control system. More thorough inspections of components would be done onshore during dry services every 2.5 years.

All components have been designed with minimal complexity so that they can be manufactured from readily available components and generic materials using basic manufacturing techniques. While there are specialist components used in this design, many could be purchased off-the-shelf or constructed and supplied separately.

3.1 Main developments and flume testing

The turbine was developed through an iterative system design process. From concept drawings, initial design calculations were formalised into a specification, designs of component parts revised in parallel and then tested with a design review. After this, designs were iterated and calculations undertaken, then tested with failure modes and effects analysis (FMEA) (Masters *et al*., 2020) and a final design loop conducted. The last stage was refinement of connections between subsystems, assembly

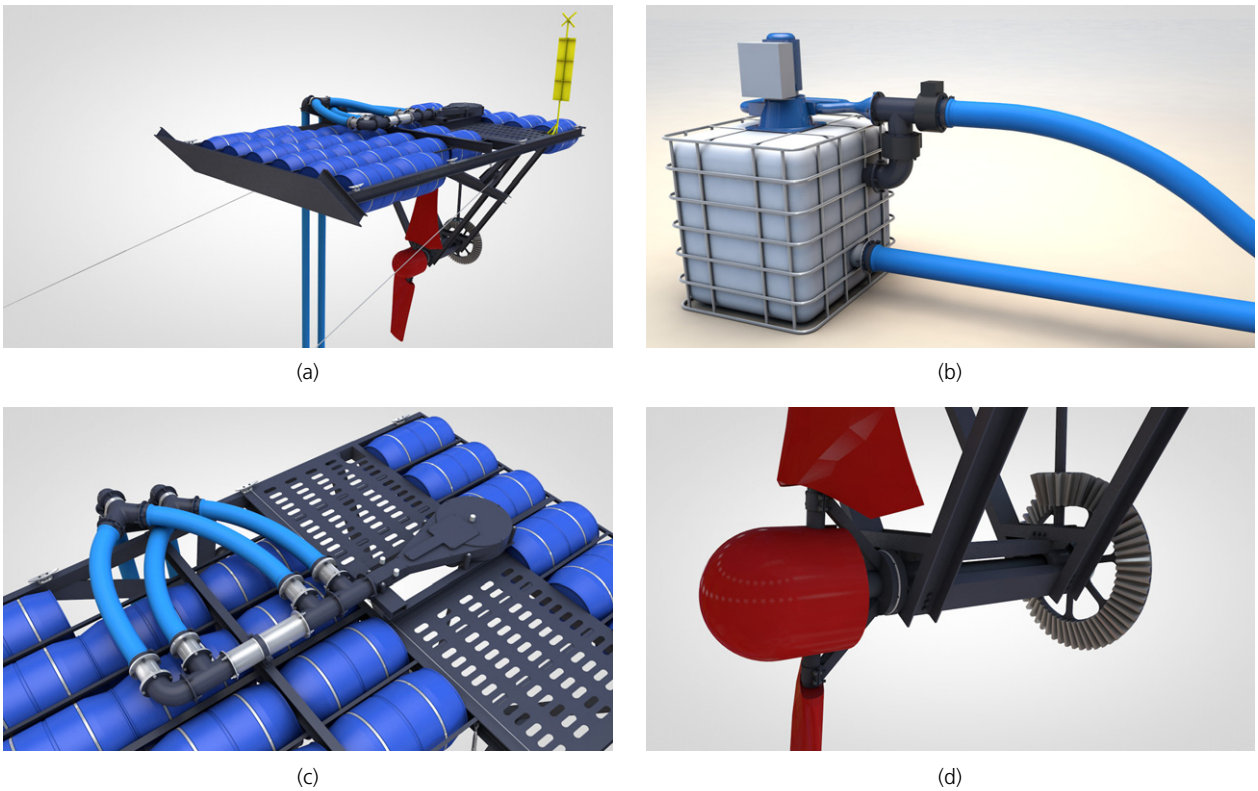

Figure 1. Computer-aided design renders of the proposed design

design and drawings. Two notable stages in the design led to significant design alterations in order to improve the functionality of the turbine. These were the completion of the FMEA and the results of a 1/50th scale model test, carried out in a flume.

The initial design iteration began by modelling the blade dynamics for a simple two-bladed rotor in the Matlab software program (detailed in Section 4.1). This gave initial blade dimensions and preliminary power, torque and thrust values to be used in the remaining component designs. During later design iterations, the PTO and control system model was developed in the Simulink software program (Section 4.2), giving the complete operating characteristics of the RRES to validate the components against. The values from the turbine loading and PTO models provided vital information for simulation and analysis of the overall design. Nodal analysis, finite-element analysis (FEA) and computational fluid dynamics (CFD) were utilised during the component design stage. These simulations were used to refine the design of individual components, and the stability of the device as a whole was tested experimentally using a flume and 1/50th scale model.

The FMEA focused on each individual component, examining how any given component could hinder the performance of the turbine or render the component or turbine inactive. Examples of changes resulting from this analysis included the introduction of a closed-loop pump system (to prevent grit from entering the piping) and the identification of quality assurance measures to be applied during manufacture, such as checking the bearings to ensure concentricity. Further details of this process and its results can be found in the report by Masters *et al.* (2020).

4. Details of the design

4.1 Initial blade dynamic calculations

The loading characteristics for a turbine 3.6 m in diameter, with a 0.5 m dia. hub, were generated using blade element momentum theory (BEMT) (Chapman *et al.*, 2013). The hub and rotor diameter were chosen to comply with the specification in Table 1. The turbine blade geometry and corresponding coefficients of power and thrust were taken from Mycek *et al.* (2014), and the lift and drag coefficients for the aerofoil section used in the design were taken from Togneri *et al.* (2020) and Zhuang *et al.* (2012), respectively.

Figure 3 shows the initial turbine design performance, with a tip speed ratio (TSR) at the optimal point for this rotor,

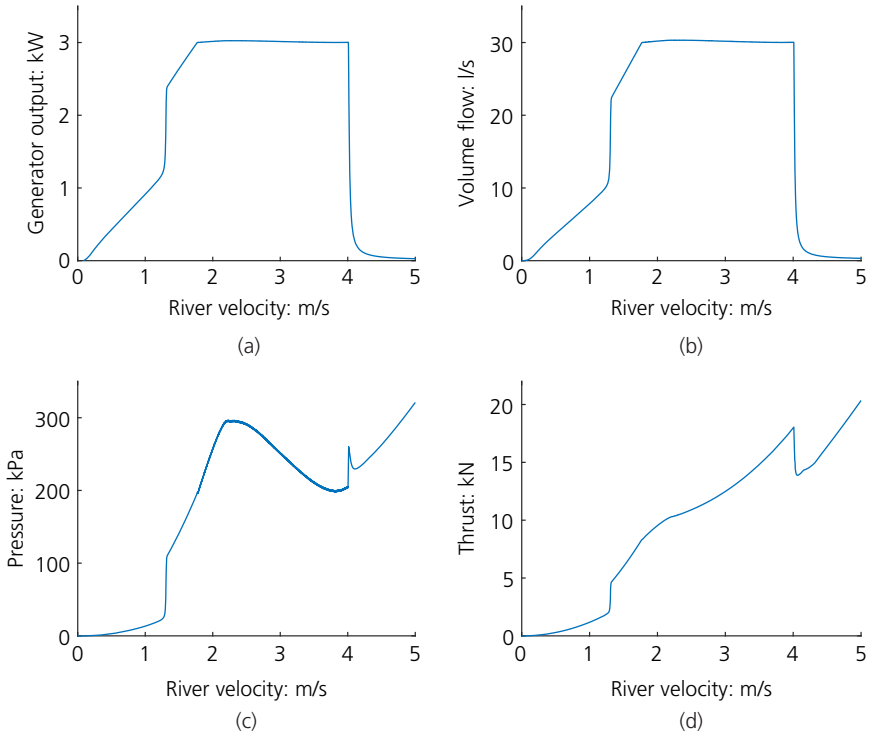

Figure 2. System performance metrics with velocity: (a) shore side electrical output, (b) pump volume flow, (c) pump pressure and (d) rotor thrust on structure

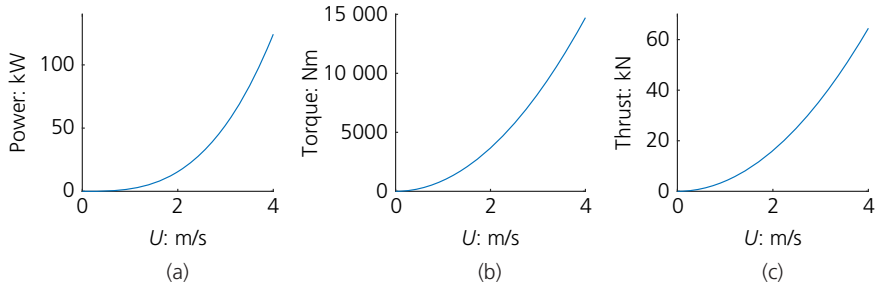

Figure 3. Power provided to the turbine (a), torque acting on the blades and hub (b), and the thrust acting on the structure (c) as the flow speed increases at optimum tip speed ratio from BEMT generated data

TSR = 3 (Edmunds *et al*., 2020; Mycek *et al*., 2014). The power, torque and thrust generated by the turbine at higher flow rates are far greater than required (Table 1). To mitigate this and reduce overall loads to a more easily managed level, a braking control system (Section 4.2) uses back pressure from the pump and generator system to maintain a constant rotational speed of 30 r/min, which is derived from the optimal TSR (Mycek *et al*., 2014). The characteristics of the turbine with this closed-loop control system applied are shown in Figure 4, which shows the variation in power and torque coefficients, C_P and C_T, with river flow speed U. The plot shows the turbine operating at optimal TSR between approximately 1.3 and 1.7 m/s, with the TSR reduced by the control system until the cut-off speed of 4 m/s is reached and the rotor is braked.

4.2 Power take off system design

The PTO system is shown in Figure 5 and includes the pump, its mechanical links to the axle, the hydro-electric generator, valves and pipework. The aim of the PTO system is to convert the

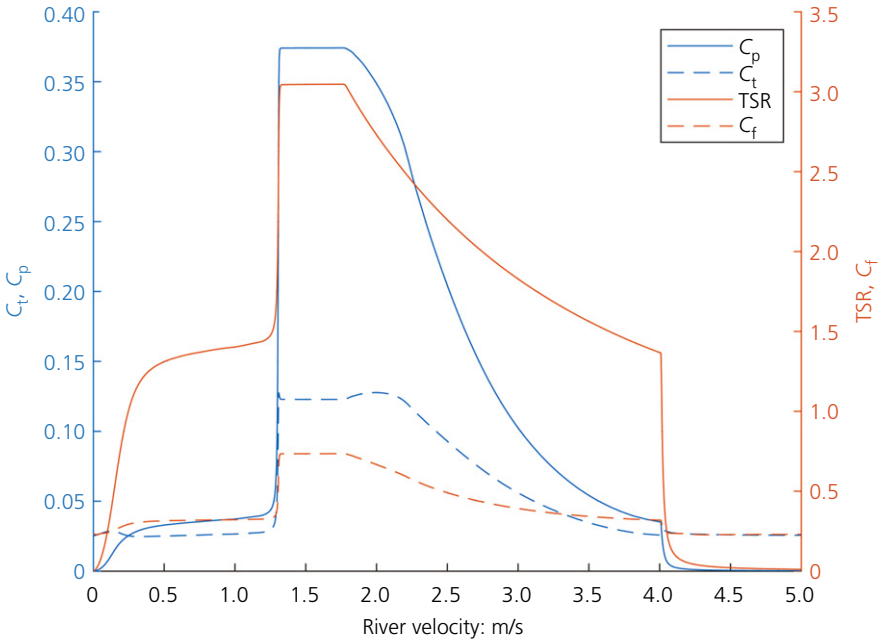

Figure 4. Plot of C_P and C_T against flow speed, including braking system effect

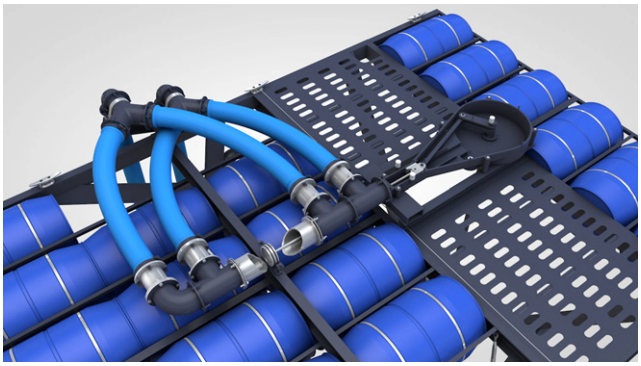

Figure 5. Renders of final PTO design offshore – with cut outs and lid removed

mechanical power of the turbine into water flow, by way of a pump, and then into electricity using a hydro-electric generator.

4.2.1 System modelling

Simulink was used to model the turbine system in detail, allowing the behaviour of the system at different river velocities to be fully quantified. An overview of the Simulink model is shown in Figure 6. The coloured regions of the model correspond to different components of the RRES design, and are discussed below.

4.2.1.1 MODEL EQUATION (PURPLE)

Equation 1 balances the torque generated by the turbine with the torque required by the pump and allows the rotational velocity, ω_r, of the turbine to be modelled at different river speeds by rearranging in terms of the angular acceleration, $d^2\theta_r/dt^2$, and integrating (Equation 2).

$$1. \quad J\frac{d^2\theta_r}{dt^2} = T_m - T_p$$

$$2. \quad \frac{d\theta_r}{dt} = \omega_r = \int (T_m - T_p)/J \, dt$$

4.2.1.2 TURBINE MODELLING (BLUE)

The mechanical torque, T_m, generated by the turbine is a function of the river velocity, rotor speed and the rotor design as discussed in Section 4.1.

4.2.1.3 PUMP MODELLING AND DESIGN (ORANGE)

The gear ratio and rotor angular velocity, ω_r, determine the pump volume flow, $\dot{V}$, which allows losses in the system to be calculated. The minor losses are given by the Darcy–Weisbach equation (Massey and Ward-Smith, 1998) (taking into account pipe, joint and valve losses) and the generator losses are modelled as a nozzle with the same characteristics. The pressure

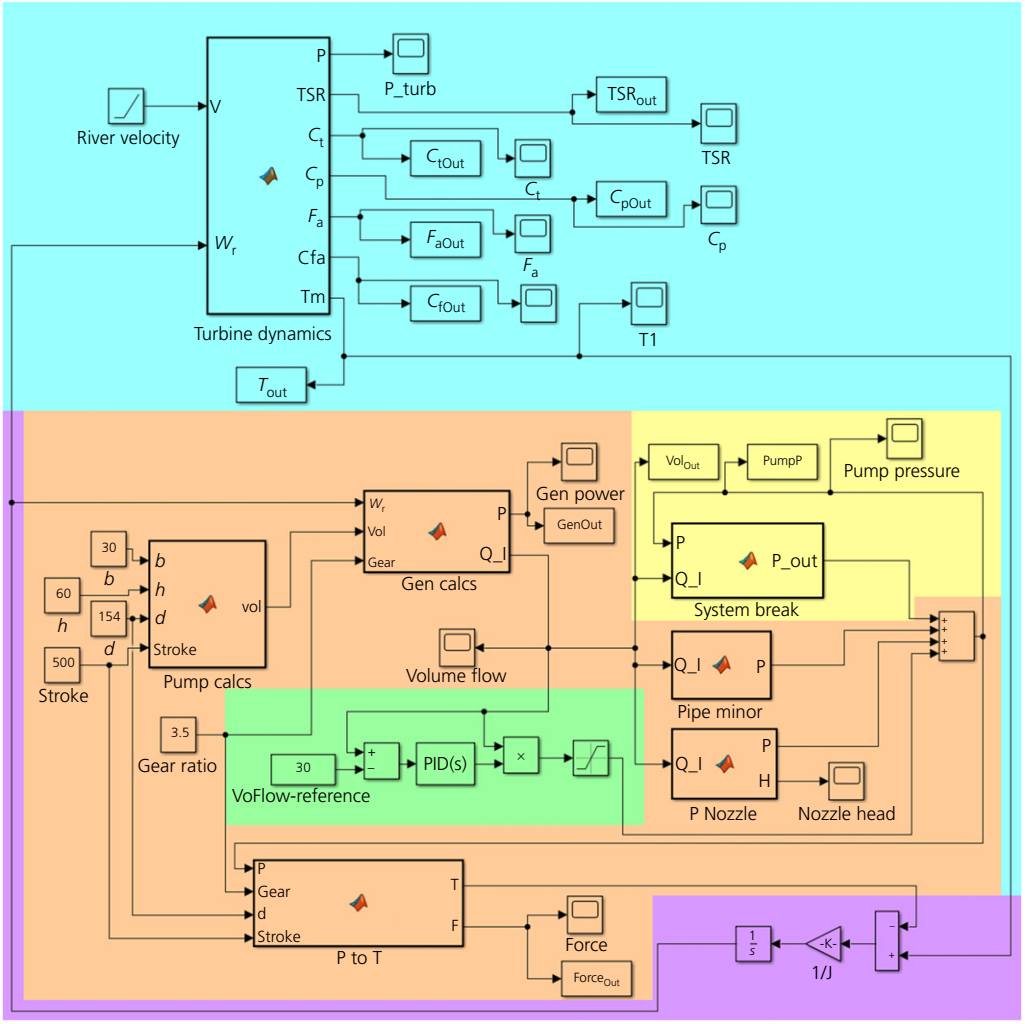

Figure 6. Simulink model of system

losses combined with the area of the piston and the crank geometry then allow the pump drive torque, T_p, to be calculated.

4.2.1.4 CONTROL SYSTEM (GREEN)

A proportional-derivative (PD) controller was used to keep the flow rate from exceeding the maximum limit by increasing the resistance to the flow using a throttling valve. This valve is part of the brake system highlighted in yellow. As flow rate is proportional to both the electrical output of the generator and the pressure loss across it, either value could be used for system control depending on the available sensors. The control system also closes the valve completely if flow rate and pressure show the river velocity is at or above 4 m/s.

4.2.1.5 MANUAL BRAKE (YELLOW)

The throttling valve used by the control system can also be closed manually to stop the rotor spinning. This could be done either in anticipation of storm water or flooding events, or to stop the turbine for maintenance.

Running the Simulink model using the values for system components described below generates the full system characteristics shown in Figure 2. The generator will output 2 kW at $U = 1.308\,\text{m/s}$ and 3 kW from $U = 1.76\,\text{m/s}$. The maximum internal pressure of the generator is 296.5 kPa at $U = 4\,\text{m/s}$. The river turbine blades are subject to a maximum thrust of 20.34 kN at $U = 4\,\text{m/s}$.

4.2.2 Design options and calculations

4.2.2.1 HYDRO-ELECTRIC GENERATOR SELECTION

The design presented here could incorporate any suitable hydroelectric generator available in a particular region; however, a single example turbine was selected in order to

illustrate the capabilities of the design. The turbine used in the modelling presented here was a 3 kW dual-nozzle generator from Suneco, based on the wide operating range and low minimum power requirement as detailed on their website (Suneco Hydro, 2020). Figure 7 provides a visual summary of the operational ranges of turbines from this manufacturer.

4.2.2.2 PIPE SELECTION

Polyethylene water pipe will be used for the turbine as it is flexible and commonly used for water. This pipe has a roughness value (ε) of 3×10^{-6} m. For the simulation, 400 m of pipe was assumed and the diameter of generator input (150 mm) was specified as the pipe diameter.

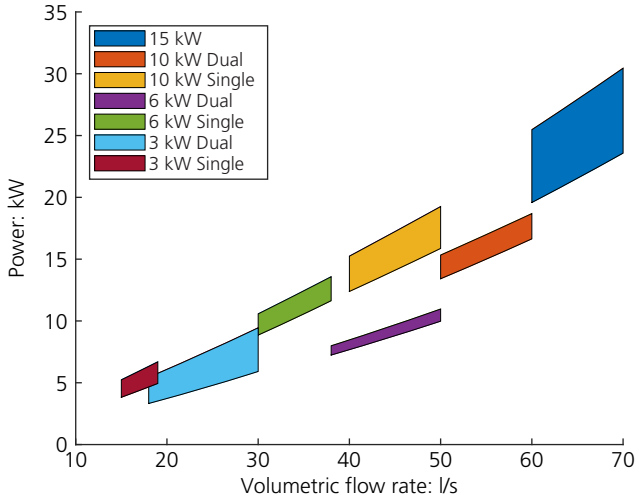

Figure 7. Input fluid power operational envelope for certain hydroelectric generators (source: based on data from Suneco Hydro (2020))

4.2.2.3 PUMP DESIGN

A dual-stroke piston system achieves consistent flow while minimising components. Section 4.1 showed the optimal C_P of the river turbine at rated current flow occurs at 30 r/min. Pump volumes calculated from the r/min range of the river turbine were considered to account for the gearing of the system. The pump volume of 17.73 l was chosen to minimise the size of the pump while maintaining a practical gear ratio and minimising the maximum force exerted on the system. Evaluating the velocity of the piston throughout each revolution of the turbine, the average flow rate was calculated as 32.58 l/s and the maximum flow rate as 54.33 l/s.

4.2.2.4 GEAR RATIO

By increasing the gear ratio between the turbine and the pump the ratio of the corresponding torques, T_m:T_p, can be adjusted. Simulation showed (Figure 8) that as the gear ratio is increased the operating torque coefficient, C_T, of the system can be kept closer to the peak value. This ensures the hydrodynamic performance peaks then decreases as the brake is applied at higher river speeds, minimising the peak torque required as the control system engages. If the gear ratio is too high, however, the mechanical torque, T_m, required to drive the pump is too high and the turbine does not spin. The optimal gear ratio was found to be around 3.6 so the pump volume was adjusted to fit a practically achievable gear ratio of 3.5.

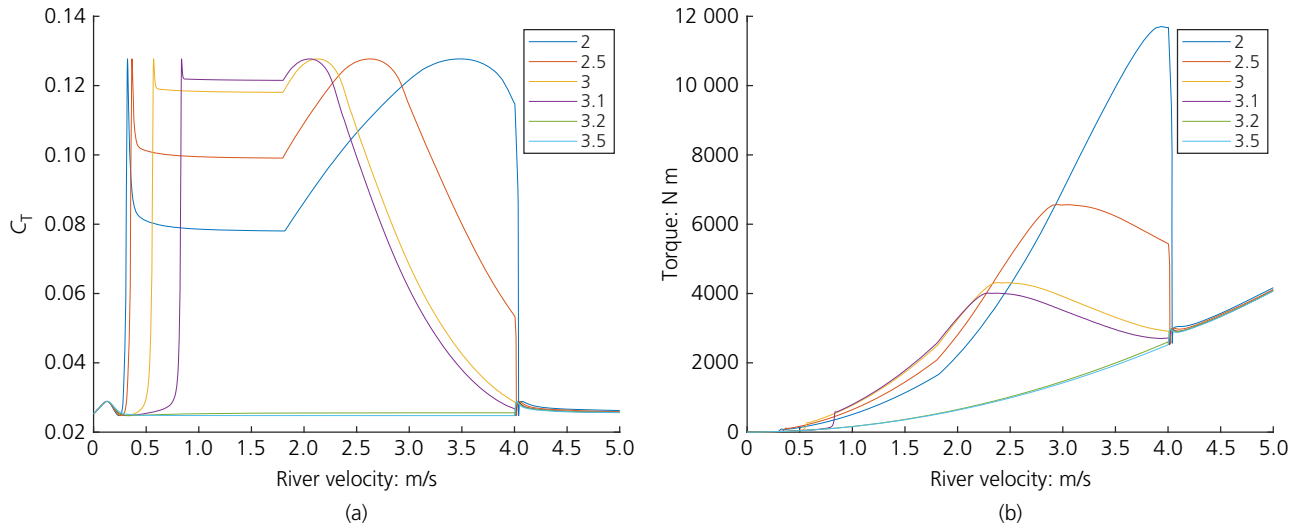

Figure 8. Effect of gear ratios on the variation of (a) C_T and (b) torque with flow speed

4.2.2.5 ONE-WAY VALVE DESIGN

To minimise the pressure losses across the pump, and also given the large internal diameter of the pipe, a one-way valve was designed to be assembled using a minimal number of specialist components. To ease the replacement of the components susceptible to wear, a flange is welded to the pipe that can then be bolted to the outlet (Figure 9).

Simulations were conducted to ensure sufficient flow through the valve with an acceptable drop of pressure across the component. A large pressure drop would reduce the efficiency of the pump system, and could risk additional wear due to cavitation (Plesset, 1949). The CFD simulation used the maximum flow rate expected through the valve, 54.33 l/s, and an inlet pressure of 400 kPa. This includes a safety factor (SF) of 1.5. A $k-\varepsilon$ turbulence model was used, as this offers an acceptable compromise between computational expense and complexity required for turbulent flows (Kim *et al*., 2001). The results of this simulation showed that the pressure would reduce by approximately 20 kPa between the valve inlet and outlet. This should not induce cavitation, and means that the valves should be operating at 95% efficiency. Additional simulations of the valve both partially open and fully closed also show that cavitation should not occur.

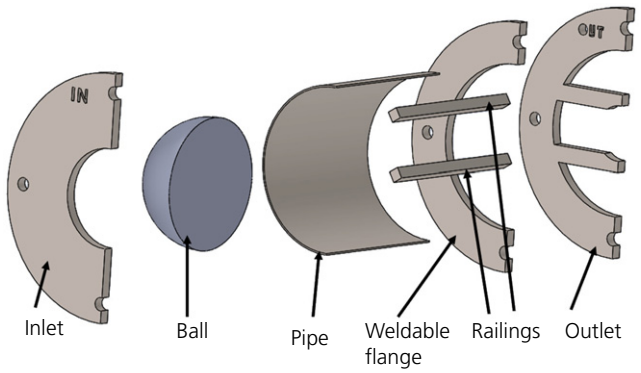

Figure 9. Exploded cross-sectional view of the one-way check valve, viewed from the inlet

4.2.2.6 CRANK ASSEMBLY DESIGN

The crank is located in a sealed chamber on top of the deck and incorporates a sliding cross head to reduce bending forces as shown on the right of Figure 5. A non-linear static FEA including mesh refinement was conducted to ensure the design was structurally sound. The maximum pressure in the system of 296.5 kPa gives a maximum force on the piston head of 5523.4 N. The final simulation (Figure 10) shows the minimum SF for this design is 2.17, above the design requirement.

4.2.2.7 BEVEL GEAR DESIGN

The PTO system is required to transfer power vertically from the turbine shaft to the pump (bidirectionally) at a gear ratio of 3.5:1. To achieve this a 3.5:1 bevel gear was selected. This was chosen over a 1:1 bevel gear and gearbox combination as the gearbox was significantly more complex, although the

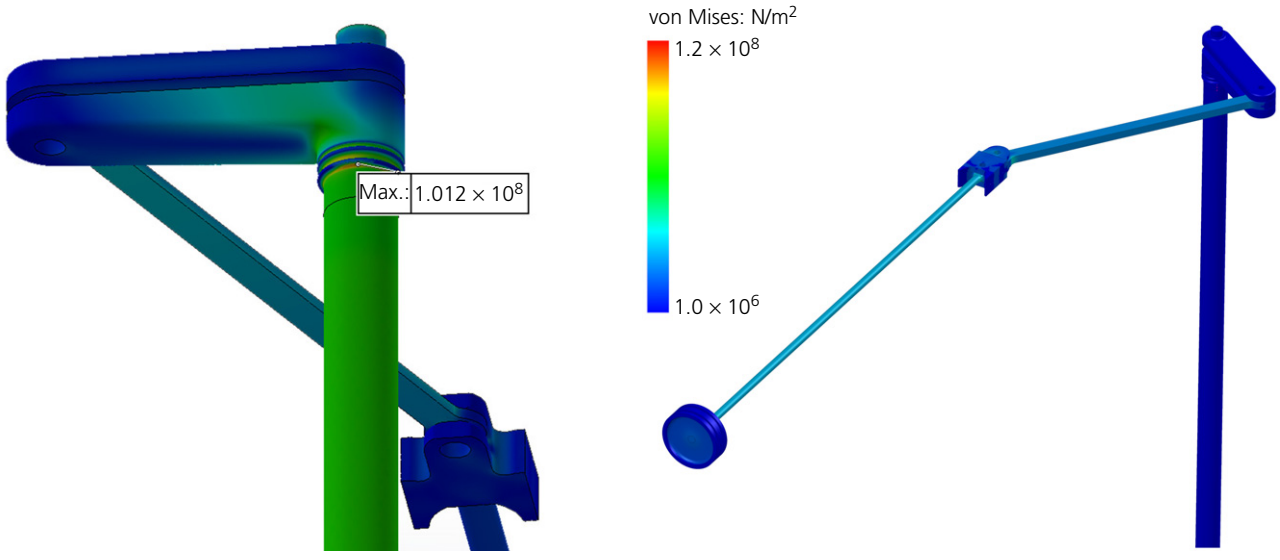

Figure 10. (a) Maximum stress location in PTO and (b) full FEA PTO results

weights of the two systems were comparable. Using force analysis and beam strength theory (Bhandari, 2010), a minimum modulus of 17.57 was calculated so the bevel gears were designed with a modulus of 18.

4.2.2.8 SEAL DESIGN

The PTO uses three sets of O-rings designed to ISO 3601-1:2008 (ISO, 2008). A pair of 434 O-rings are used on the piston, three 116 O-rings are used on the piston rod to separate the water and oil sections and a 141 O-ring is used to mitigate ingress into the lower bearing. The top of the pump will use a 0.4 mm gasket and the inspection cover will use a rubber seal.

4.2.2.9 MATERIAL SELECTION

Material selection was based on the requirements to mitigate corrosion, minimise cost and be easy to machine. Due to the potential surface wear from the seals, a coating could not be used on the piston or piston rod so they will be made from stainless steel. These components will be electrically insulated from the remainder of the PTO system using nylon inserts, gaskets and washers to prevent galvanic corrosion (Bouzid *et al*., 1995; Zhang, 2011). The designed one-way valves will be made from stainless steel, with a polycarbonate ball, as both offer a long working life and are recyclable (Gordon *et al*., 2006; Liu *et al*., 2017; Payet-Gaspard, 2012). The ball needs to move freely within the valve, and the use of polycarbonate gives it a density similar to water – in this case the specific gravity of the polycarbonate ball is 1.2, meaning it is nearly neutrally buoyant (Khurshudov and Kato, 1997; Utracki and Sammut, 1990). The crank casing will be made from cast iron and all remaining components will be made from carbon steel.

4.3 Bearing design

To keep the manufacture of the bearing components simple, designs requiring bearing seals were excluded at an early stage. Journal bearings have been designed, rather than ball or roller bearings, which reduces the number of moving parts and allows for larger clearances. The larger clearances reduce the vulnerability of the bearings to interference caused by sedimentation.

A preliminary observation of some lubrication regime graphs showed that for the design envelope of a maximum r/min of around 25–30, hydrodynamic lubrication would not be reached unless an impractically large shaft diameter was used (Welsh, 1983). Hydro-static lubrication was also deemed infeasible, as it required the pump to already be in motion in order to lift the bearing surface enough to create a suitable oil wedge. This requires that the bearings operate in a boundary-lubricated regime. As such, flat-plate thrust bearings and plain journal bearings were designed for the blade shaft. The loads on the main shaft bearings are shown in Figure 11, with the thrust forces created by the blades acting against the relatively large front thrust bearing and a second thrust bearing at the rear of the shaft, providing a contact surface for the rear bevel gear.

4.3.1 Design and calculations

The methodology used to obtain the geometry of the thrust bearings is detailed by Wilcock and Booser (1957b). Bearing sizing calculations were carried out using an early estimate of thrust load, with $W_{th} = 23\,\text{kN}$. The outer diameter of a thrust bearing can be calculated using Equation 3, where the meaning and units of each variable are stated in the notation list.

$$3. \quad D_2 = \left(\frac{4W_{th}}{\pi k_g P_{th}} + D_1^2\right)^{1/2}$$

Normal pressure loads for flat plate thrust bearings should be kept to below 75 psi (517 kPa), with the maximum loads being less than 150 psi (Wilcock and Booser, 1957b). Using an SF of 2, a design target P value of 517 kPa is taken. The pad/circumference ratio, k_g, is usually given as 0.8. Given that both D_1 and D_2 are unknown, an iterative process was used to

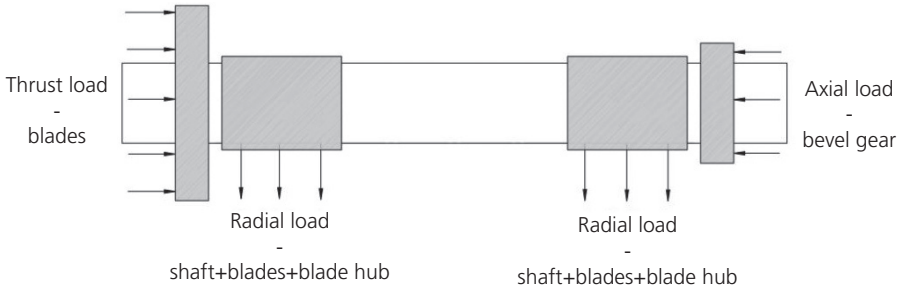

Figure 11. Bearing load diagram

find suitable values that would satisfy the general criteria given in Equation 4. The final D_1 value also defines the shaft diameter.

4. $$1.5D_1 < D_2 < 2.5D_1$$

Additional geometries including b, i, B and G may be calculated using Equations 5–8. The rear thrust bearing was designed using the same dimensions as that of the front, as this avoids assembly errors that could be caused by interchanging the two parts.

5. $$b \approx \frac{D_2 - D_1}{2}$$

6. $$i = \frac{\pi}{2} k_g \left(\frac{D_1 + D_2}{b} \right)$$

7. $$B \approx \pi k_g \left(\frac{D_1 + D_2}{2i} \right)$$

8. $$G \approx 0.2B$$

The power loss due to each thrust bearing can be estimated by first calculating U_d using Equation 9. A U_d value of 16 mm/min can be reached for the front thrust bearing (under the greatest load). An estimate for M can then be found by comparing with past data values of U_d (Wilcock and Booser, 1957b), resulting in $M \ll 0.1$. The actual power loss is found using Equation 10, indicating that the power loss due to the thrust bearings is negligible.

9. $$U_d = \frac{\pi}{24} (D_1 + D_2) \frac{\omega_{rev}}{60}$$

10. $$H = ibBM$$

4.3.1.1 JOURNAL BEARING CALCULATIONS

Using the inner diameter determined by the thrust bearings, L_{jo} can be determined using the standard L:D ratio of 0.5:1.5. P_{jo} is given in Equation 11 (Childs, 2013), where W_{jo} is assumed to be approximately equal to 100 kg (140 kg after applying the partial SF of 1.4). C is subsequently given in Equation 12 (O'Connor *et al*., 1968).

11. $$P_{jo} = \frac{W_{jo}}{L_{jo} D_1}$$

12. $$2C = 0.001D_1 + 0.001$$

The bearing thickness is found using Equation 13 (Berard and Waters, 1924). A Stribeck curve can be used to estimate the friction factor of journal bearings based on their lubrication regime, or more accurately by using their Hersey number as calculated using Equation 14 (Williams, 2004). In this case, a Hersey number of 0.009 corresponds to a friction factor of around 0.1 as expected. This is consistent with friction factors of around 0.08−0.1 for typical boundary-lubricated bearings.

13. $$t = 0.3D + 1.25$$

14. $$\text{Hersey number} = \frac{\eta}{P} \frac{\omega}{60}$$

A rough estimate of friction factor for partially lubricated bearings can be calculated using Equation 15, where V is calculated as shown in Equation 16 and C_1 and C_2 are constants that depend on the bearing's operating conditions and type, respectively (Vallance, 1938). This results in a friction factor, f, of 0.135 under ordinary conditions. A worst-case scenario with major sedimentation interference would increase this to 0.27.

15. $$f = \frac{C_1 C_2}{250} \left(\frac{P_{jo}}{V} \right)^{1/4}$$

16. $$V = \frac{\pi D_1 \omega_{rev}}{12}$$

4.3.1.2 MATERIAL SELECTION AND MANUFACTURING

Given that the very low r/min creates a dry rubbing condition at times and considering the relatively low loading conditions of the RRES, a plastic material with low dry friction coefficient was chosen for the bearings. Plastics also have the benefit of being softer than the steel shaft journal material. This is useful when considering particulate interaction with the bearing

– there is no filtration in the system so there is potential for particulates to enter the bearing and damage the shaft surface. The softer interface material can be regarded as sacrificial, protecting the more expensive shaft (Williams, 2004). Nylon could be used, which is cheap (Wilcock and Booser, 1957b), tough and easier to machine, while polytetrafluoroethylene (PTFE) has a lower coefficient of friction, better chemical resistance and higher operating temperatures (Freeman, 1962; Wilcock and Booser, 1957a). The most important characteristic for the RRES bearings is the material wear rate, considering the desire

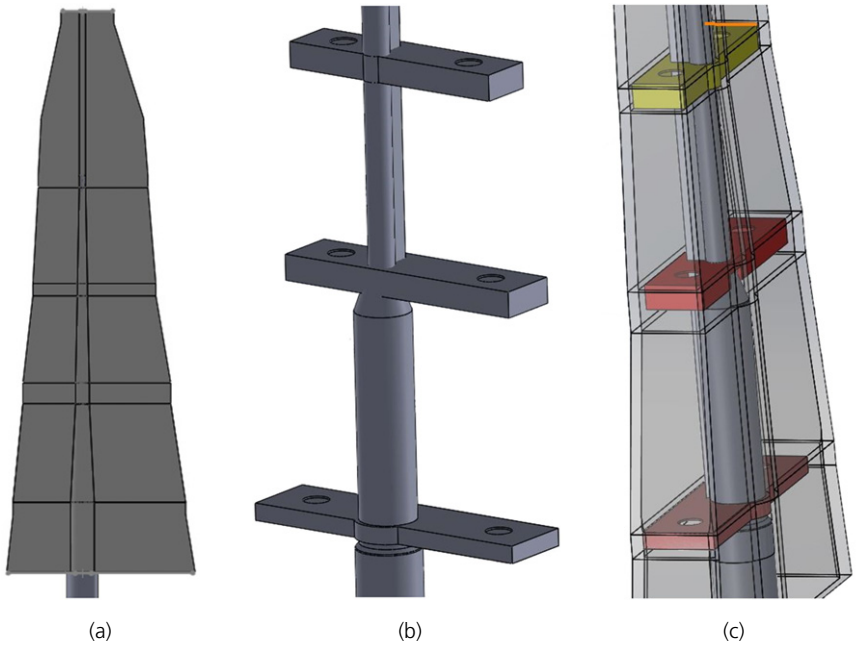

Figure 12. (a) Simplified blade geometry for analysis, (b) spar caps and (c) full assembly

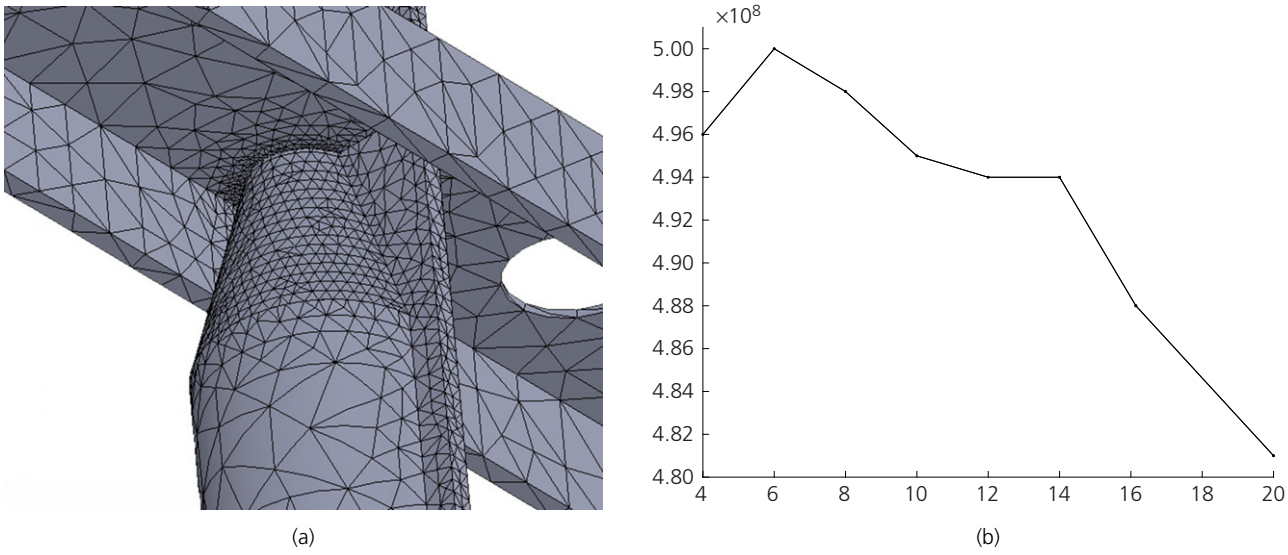

Figure 13. (a) Mesh refinement in high-stress area and (b) graph of mesh refinement steps

for longer design life and the expectation of sedimentation interference. For these reasons, PTFE was selected (Zsidaia *et al*., 2002).

4.4 Blade structural design

Development of the blade structure was designed to fulfil the requirements set out in Table 1. The blade dimensions are scaled up from Mycek *et al*. (2014) with a new radius of 1.8 m, maximum chord length of 0.223 m and a minimum of 0.0590 m using a National Advisory Committee for Aeronautics (NACA) 63418 profile. In line with the requirement that the design must use common materials, simple manufacturing methods and must be easily repaired, an open-mould, wet-layup fibreglass process is proposed.

The design was verified using a static load simulation in the Solidworks software program. The thrust was applied to the face of the blade in the direction of the axis of rotation. To simplify the geometry, a basic blade was modelled with the same thickness and approximate shape as the actual blade. This is shown in Figure 12(a). The internal geometry is shown in Figures 12(b) and 12(c). Under the assumption that the control system fails to bring the rotor under control in storm conditions, the maximum thrust load is 60 000 N (Figure 3), split between the two blades. This was multiplied by an SF of 3.3 as suggested in the small wind turbine design standard IEC61400-2 (IEC, 2013) to include an allowance for fatigue effects, meaning no additional fatigue analysis is required. A mesh refinement was conducted on the final assembly, shown in Figure 13, and results from the FEA showing the stress distribution for the blade and support structure are presented in Figure 14. Figure 15 shows an exploded view of the rotor assembly. To ensure easy replacement of the blades, it is mostly bolted together.

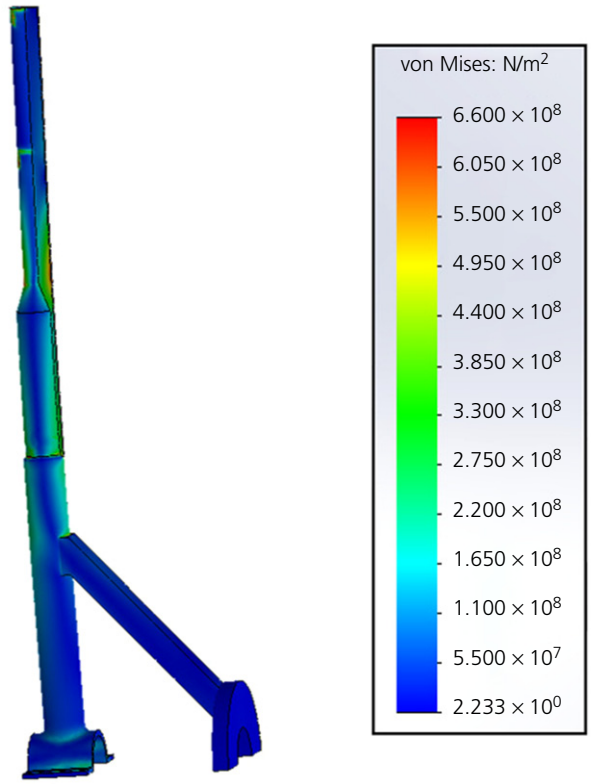

Figure 14. Final stress plot for 82.5 kN load

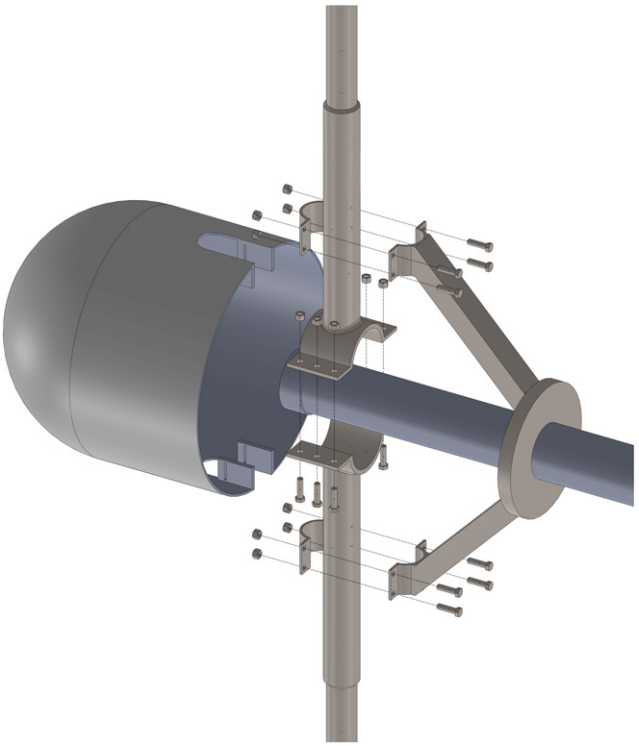

Figure 15. Exploded view assembly

4.5 Chassis design

The chassis holds all components together and provides buoyancy, mooring points and shaft housing. As noted in the design specification, this must be designed for reliability, ease of manufacture and repair, and for low cost. The main framework has been designed for manufacture from readily available standard beams using only welding and bolted joints to assemble.

Decommissioned plastic barrels (210 l) filled with closed-cell expanding foam are used for buoyancy – the foam ensuring that the barrels retain their buoyancy even when damaged. They fully cover the turbine below, so boats can approach the

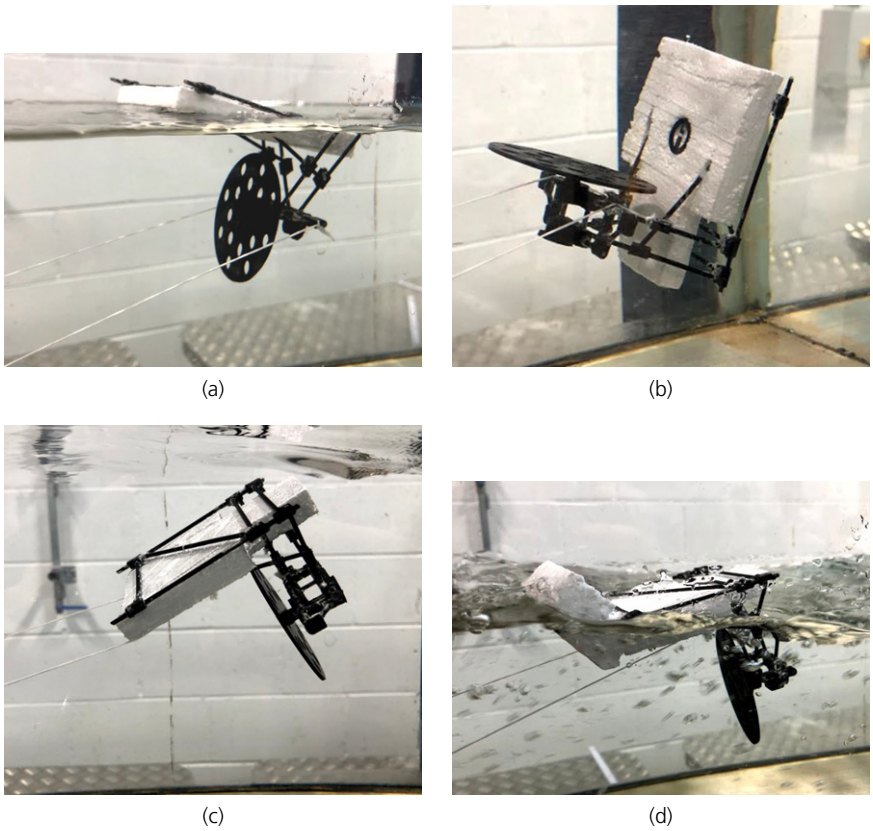

Figure 16. Flume testing of 1:50 scale models: the original design in (a) low and (b) medium flow speeds. Initial revision in a stable but partially submerged position (c), and the final revision in (d)

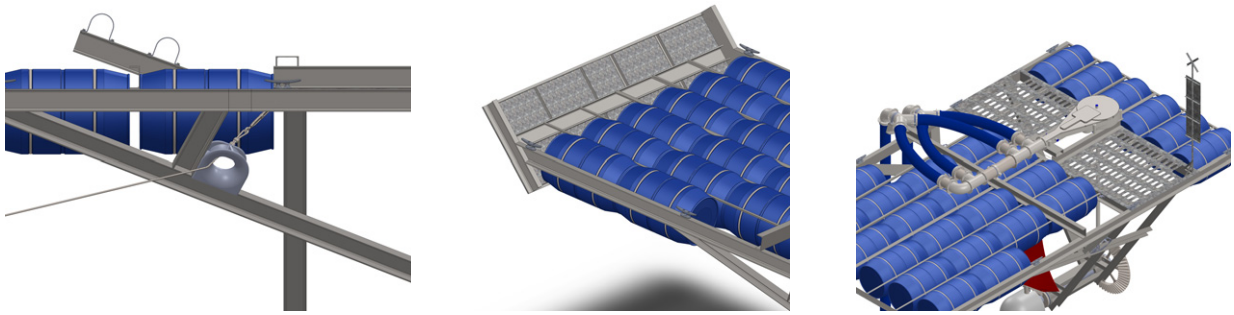

Figure 17. Design changes made after the flume testing: (a) revised mooring points, (b) bow plate and additional barrels, (c) additional rear buoyancy

sides. Treating the underside of the RRES chassis as a flat plate allows the boundary layer flow between the chassis and blades to be calculated. Setting the gap between the turbine blade tip and chassis to 250 mm ensures that as the blade passes this region, the flow into the turbine is no less than 90% of the river speed, U, up to flow speeds of 2 m/s.

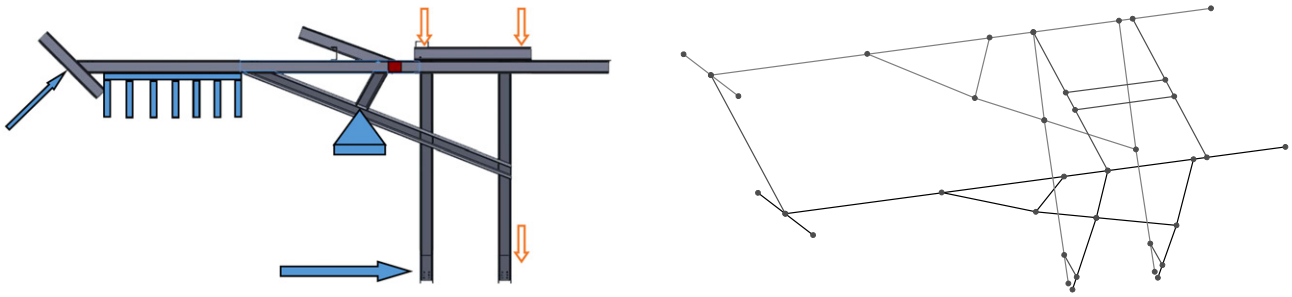

Figure 18. Structural analysis models: (a) free-body diagram, (b) Staad Pro nodal analysis

The RRES is suspended in the river flow by two mooring lines for stability and simplicity in one-directional flow; in accordance with DNVGL-OS-E304 offshore mooring standard (Lohne, 1996). Woven steel wire rope and spiral steel strand rope were considered. Spiral strand was selected to ensure longevity for applications across the 10–20 year time frame as the flexibility of the woven steel rope was not necessary for this application (Sefton *et al*., 1998). The SF of lines and anchors must be at least 3, in the scenario where one fails the other must still function under the entire design load, tethering the RRES until a crew arrives. These mooring lines shall pass through the chocks (mooring line guide-holes) to a turnbuckle wire tension device which in turn is fixed by the deck, which allows the mooring to be adjusted to angle the turbine into the flow. The steel chocks shall have a bolt-in chock liner to protect the lines from wear at this most crucial point (Taylor and Hawkins, 2000).

4.6 Flume testing alterations

An open-channel, 300 mm wide, hydraulic flume was used for the test to improve the design of the chassis as shown in Figure 16. A 1/50th scale model of the chassis was made with wire and three-dimensional-printed lugs using polystyrene as buoyancy for flume testing. To replicate the drag loads from the rotor, the actuator disc approach of Myers and Bahaj (2010) was used and a disc with 42% porosity was manufactured.

The flume testing proved to be a crucial development step as it showed that, when moored from a brace as shown in Figure 16(a) in high flow, the structure could invert as shown in Figure 16(b). From the tests it was concluded that the mooring lines should be attached above and forward of the turbine position, resulting in the stable configuration shown in Figure 16(c). This configuration is stable even in adverse conditions, but meant that the bow of the RRES would dive underwater in high flow rates, which was resolved with a bow structure (Figure 16(d)).

The final design with these revisions incorporated is shown in Figure 17.

4.6.1 Material strength

The structural strength was verified using truss nodal analysis and to determine which size of the C-section beams are used. The thrust load on the turbine, buoyancy and weight of the pump and gear system are shown in the free-body diagram (FBD) in Figure 18(a). Staad Pro nodal analysis is shown in Figure 18(b). Five C-beams were tested. All of these were standard dimensions from the UPE series defined by BS EN 10365 (BSI, 2017): UPE 140, 160, 180, 200 and 220. The UPE 160 option gave the lightest weight and an SF of 2.

5. Conclusions

This turbine design will provide electrical power for a remote location. The design envelope encompasses water speeds between 1 and 4 m/s and rated power of 3 kW from a river flowing at 1.8 m/s. The design concept has been refined to minimise the use of complex manufacturing techniques, and to use materials that are widely available. There are no electronics off-shore, minimising the complexity of maintenance. The turbine, pump and chassis systems are completely mechanical, pumping water on-shore to power a generator. This can accommodate the use of a throttling system to prevent the turbine entering an overspeed state and exceeding design limits. The publication of the designs under an open license allows for the future development and deployment of the turbine wherever it is needed.

A 1/50th scale model was tested together with a variety of simulation techniques to validate the different component designs, including CFD, nodal analysis and FEA.

Therefore, this paper has shown a new potential direction for the provision of electricity in remote areas. The design encourages local ownership and local engagement with the technology and could be a truly sustainable solution.

Acknowledgements

This work has been supported in part by two Engineering and Physical Sciences Research Council (EPSRC)-funded Supergen ORE project grants: SURFTEC grand challenge project EP/N02057X/1 and WTIMTS flex fund project EP/S000747/1.

REFERENCES

Al-Bahadly I (2009) Building a wind turbine for rural home. *Energy for Sustainable Development* **13(3)**: 159–165.

Anyi M, Kirke B and Ali S (2010) Remote community electrification in Sarawak, Malaysia. *Renewable Energy* **35(7)**: 1609–1613.

Bansal R, Zobaa AF and Saket R (2005) Some issues related to power generation using wind energy conversion systems: an overview. *International Journal of Emerging Electric Power Systems* **3(2)**: article 1, https://doi.org/10.2202/1553-779X.1070.

Berard S and Waters E (1924) *The Elements of Machine Design*. Blackie and Son Limited, London, UK.

Bhandari V (2010) *Design of Machine Elements*. Tata McGraw-Hill Education, London, UK.

Boddapati V and Daniel SA (2020) Performance analysis and investigations of grid-connected solar power park in Kurnool, South India. *Energy for Sustainable Development* **55**: 161–169.

Bouzid A, Chaaban A and Bazergui A (1995) The effect of gasket creep-relaxation on the leakage tightness of bolted flanged joints. *Journal of Pressure Vessel Technology* **117(1)**: 71–78.

BSI (2017) BS EN 10365:2017: Hot rolled steel channels, I and H sections. Dimensions and masses. BSI, London, UK.

Castro FA and Chiang LE (2020) Design optimization and experimental validation of a two-body wave energy converter with adjustable power take-off parameters. *Energy for Sustainable Development* **56**: 19–32.

Chapman J, Masters I, Togneri M and Orme J (2013) The Buhl correction factor applied to high induction conditions for tidal stream turbines. *Renewable Energy* **60**: 472–480.

Childs P (2013) *Mechanical Design Engineering Handbook*. Elsevier, London, UK.

Edmunds M, Williams AJ, Masters I, Banerjee A and VanZwieten JH (2020) A spatially nonlinear generalised actuator disk model for the simulation of horizontal axis wind and tidal turbines. *Energy* **194**: 116803, https://doi.org/10.1016/j.energy.2019.116803.

Freeman P (1962) *Lubrication and Friction*. Sir Isaac Pitman & Sons Ltd, London, UK.

Gordon RB, Bertram M and Graedel TE (2006) Metal stocks and sustainability. *Proceedings of the National Academy of Sciences* **103(5)**: 1209–1214.

Griggs D, Stafford-Smith M, Gaffney O *et al.* (2013) Policy: Sustainable development goals for people and planet. *Nature* **495(7441)**: 305–307.

IEC (International Electrotechnical Commission) (2013) *Wind Turbines – Part 2: Small Wind Turbines. Standard IEC 61400-2:2013*. International Electrotechnical Commission, Geneva, Switzerland.

ISO (International Organization for Standardization) (2008) ISO 3601-1:2008: Fluid power systems — O-rings — Part 1: Inside diameters, cross-sections, tolerances and designation codes. ISO, Geneva, Switzerland.

Khurshudov A and Kato K (1997) Wear mechanisms in reciprocal scratching of polycarbonate, studied by atomic force microscopy. *Wear* **205(1–2)**: 1–10.

Kim CS, Kim C and Rho OH (2001) Sensitivity analysis for the Navier-Stokes equations with two-equation turbulence models. *AIAA Journal* **39(5)**: 838–845.

Kirke B (2019) Hydrokinetic and ultra-low head turbines in rivers: a reality check. *Energy for Sustainable Development* **52**: 1–10.

Liu Y, Zhou H, Guo JZ, Ren WM and Lu XB (2017) Completely recyclable monomers and polycarbonate: approach to sustainable polymers. *Angewandte Chemie International Edition* **56(17)**: 4862–4866.

Lohne P (1996) *Certification of Offshore Mooring Steel Wire Ropes. Technical Report*. American Society of Mechanical Engineers, New York, NY, USA.

Massey BS and Ward-Smith J (1998) *Mechanics of Fluids*. CRC Press, Boca Raton, FL, USA, vol. 1.

Masters I, Bird J, Birch B *et al.* (2020) *Remote River Energy System. Technical Report*. Swansea University, Swansea, UK.

Mycek P, Gaurier B, Germain G, Pinon G and Rivoalen E (2014) Experimental study of the turbulence intensity effects on marine current turbines behaviour. Part I: one single turbine. *Renewable Energy* **66**: 729–746.

Myers L and Bahaj A (2010) Experimental analysis of the flow field around horizontal axis tidal turbines by use of scale mesh disk rotor simulators. *Ocean Engineering* **37(2–3)**: 218–227.

O'Connor J, Boyd J and Avallone E (1968) *Standard Handbook of Lubrication Engineering*. McGraw-Hill, New York, NY, USA.

Orme JC and Masters I (2005) Design and testing of a direct drive tidal stream generator. *Proceedings of the Institute of Marine Engineering, Science and Technology. Part B, Journal of Marine Design and Operations* **9**: 31–36.

ORPC (Ocean Renewable Power Company) (2020a) *Ocean Renewable Power Company (ORPC)*. ORPC, Portland, ME, USA. See https://www.orpc.co/ (accessed 24/03/2020).

ORPC (2020b) *Ocean Renewable Power Company: Remote Communities*. ORPC, Portland, ME, USA. See https://www.orpc.co/markets/remote-communities (accessed 24/03/2020).

OSHWA (Open Source Hardware Association) (2020) *Definition (English)*. OSHWA, Boulder, CO, USA. See https://www.oshwa.org/definition/ (accessed 22/02/2022).

Payet-Gaspard P (2012) Stainless steel and sustainability. *La Metallurgia Italiana* **5**: 57–60.

Plesset MS (1949) The dynamics of cavitation bubbles. *Journal of Applied Mechanics* **16(3)**: 277–282.

Razmjoo A, Shirmohammadi R, Davarpanah A, Pourfayaz F and Aslani A (2019) Stand-alone hybrid energy systems for remote area power generation. *Energy Reports* **5**: 231–241.

Sefton S, Firth K and Hallam S (1998) *Installation and Handling of Steel Permanent Mooring Cables*. Bridon International, Doncaster, UK.

Smart Hydro Power (2015) *Smart Monofloat Turbine*. Smart Hydro Power, Feldafing, Germany. See https://www.smart-hydro.de/renewable-energy-systems/hydrokinetic-turbines-river-canal/ (accessed 24/03/2020).

Smart Hydro Power (2016) *Smart Riverbed Turbine*. Smart Hydro Power, Feldafing, Germany. See https://www.smart-hydro.de/renewable-energy-systems/hydrokinetic-turbines-river-canal/ (accessed 24/03/2020).

Suneco Hydro (2020) *Hydro Turbine Generator, Water Turbine Generator from 300W to 6000KW*. Suneco Hydro, Beijing, China.

See https://www.micro-hydro-power.com/hydro-turbine-generator/ (accessed 24/03/2020).

Taylor CF and Hawkins CA (2000) Cargo chock. US Patent 6,012,885, Oct.

The World Bank Group (2009) *Energy Strategy Approach Paper: Main Report (English). Technical Report*. The World Bank Group, Washington, DC, USA. See http://documents.worldbank.org/curated/en/833051468161084224/Main-Report (accessed 22/02/2022).

Togneri M, Pinon G, Carlier C, Bex CC and Masters I (2020) Comparison of synthetic turbulence approaches for blade element momentum theory prediction of tidal turbine performance and loads. *Renewable Energy* **145**: 408–418.

Tong W (2010) *Wind Power Generation and Wind Turbine Design*. WIT Press, Southampton, UK.

UN (1987) *Report of the World Commission on Environment and Development: Our Common Future*. UN, New York, NY, USA.

Utracki L and Sammut P (1990) Rheology of polycarbonate/linear low density polyethylene blends. *Polymer Engineering & Science* **30(17)**: 1027–1040.

Vallance A (1938) *Design of Machine Members*. McGraw-Hill, London, UK.

Welsh R (1983) *Plain Bearing Design Handbook*. Butterworths, Oxford, UK.

Wilcock D and Booser E (1957a) *Bearing Design and Application*. McGraw-Hill, London, UK.

Wilcock D and Booser E (1957b) *Fundamentals of Machine Component Design*. McGraw-Hill, London, UK.

Williams J (2004) *Engineering Tribology*. Cambridge University Press, Cambridge, UK.

Zhang XG (2011) Galvanic corrosion. In *Uhlig's Corrosion Handbook* (Revie RW (ed.)). Wiley, Hoboken, NJ, USA, pp. 123–143.

Zhuang Y, Sun X, Huang D and Wu G (2012) Numerical study on aerodynamic performances of the wind turbine rotor with leading-edge rotation. *Journal of Renewable and Sustainable Energy* **4(6)**: 063103.

Zsidaia L, De Baetsb P, Samynb P *et al.* (2002) The tribological behaviour of engineering plastics during sliding friction investigated with small-scale specimens. *Wear* **253(5–6)**: 673–688.